Chapter 3 Characterizations

3.1 Introduction

The aim of this thesis is to develop synthetic methods for preparing bimodal micro-/meso-porous MOF nanocrystals, uniform nanosized MOFs with controlled shape and size and subsequently, the extensive application of the prepared nanosized MOFs. To accomplish this work, X-ray diffraction (XRD); electron microscopy techniques including scanning electron microscopy (SEM), transmission electron microscopy (TEM) and the complementary energy dispersive X-ray spectroscopy (EDS); X-ray photoelectron spectroscopy (XPS); Fourier transform infrared spectroscopy (FTIR); ultraviolet-visible spectroscopy (Uv-vis); ζ-potential analysis; thermal analysis including thermogravimetric analysis (TGA) and differential thermal analysis (DTA); atomic absorption spectroscopy (AAS); gas adsorption and gas chromatography (GC) have been used for characterizations. In this chapter, the principles of the characterizations are outlined. The details on the experiments are presented in the following chapters.

3.2 X-ray diffraction

X-ray diffraction is a powerful technique in the analysis of crystalline solids and mesoporous materials. This techique provides valuable information on the phase structure of crystals and the pore array of mesostructures.

The wavelength of X-ray lies in the Ångstrøm-sized range which is similar to the distance between atoms in solids.[1] When X-rays enter a crystal, the lattice planes of the crystal can cause constructive and destructive interferences of the scattered X-rays. According to Bragg's law, the constructive interference that generates diffraction peaks is obtained when the path difference of the scattered X-rays is a multiple integer of the X-ray wavelength:

$$n\lambda = 2d\sin\theta \tag{3-1}$$

Where n is the order of interference

λ is the wavelength of X-ray

d is lattice plane distance

θ is the angle of incidence

When θ is known, the distance between the lattice planes can be easily deduced.

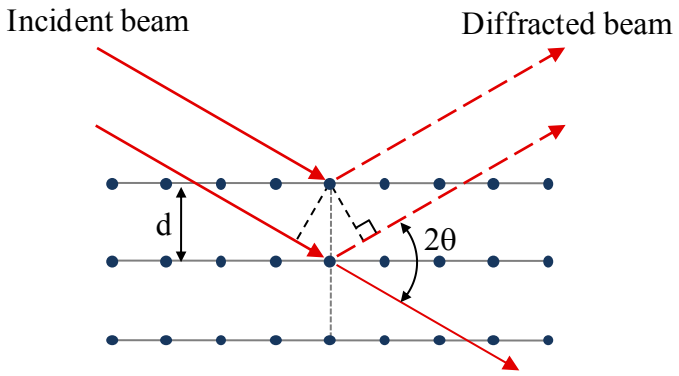

Figure 3.1 Schematic illustration of the Bragg's law.

The Debye-Scherrer equation can be applied to calculate the mean size of crystals from XRD pattern:

$$D = \frac{K\lambda}{\beta\cos\theta} \tag{3-2}$$

Where D is crystal size

K is Scherrer constant, in general set to 0.9

λ is the wavelength of X-ray

β is full width at half maximum in radians

θ is the angle of incidence

Although the mesoporous materials are usually not crystalline at atomic level, the periodic pore structure in a long range can cause the interferences of the scattered X-rays in the same way of crystalline structure (Figure 3.1 and Figure 3.2). However, due to their long range regularity in the nanometer scale, the diffraction takes place at low range of the 2θ angle, generating small angle X-ray scattering (SAXS) pattern. Since the mesopore diameter (d_{pore}) can be determined from the pore size distribution by nitrogen adsorption-desorption isotherm analysis, the wall thickness (t_w) can be calculated by following equation:

$$t_w = a_o - d_{pore} \qquad (3\text{-}3)$$

Where a_o is the distance between the centers of two adjacent mesopores, and can be deduced from d-spacings.

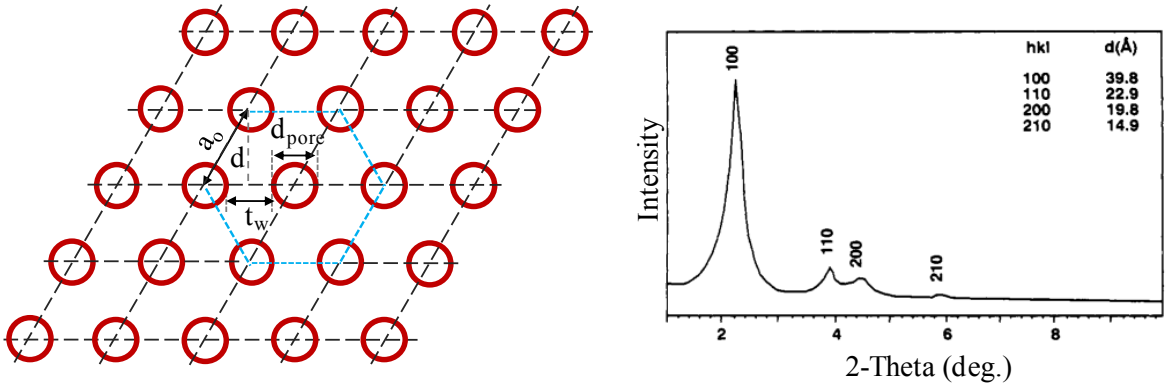

Figure 3.2 Scheme of a long-range hexagonal order in mesoporous materials (left) and SAXS pattern of the representative mesoporous material MCM-41 (righ).[2]

3.3 Electron microscopy

Electron can be considered as a wave with a short wavelength. The wavelength of electrons accelerated by high voltage is much smaller than that of visible light. Therefore, the accelerated electrons allow imaging on small scales. The SEM and TEM are commonly used microscopy techniques.[3,4] These techniques use an electron optical system to produce

a fine electron beam with high energy. The high-energy electron beam is then focused onto solid specimen.

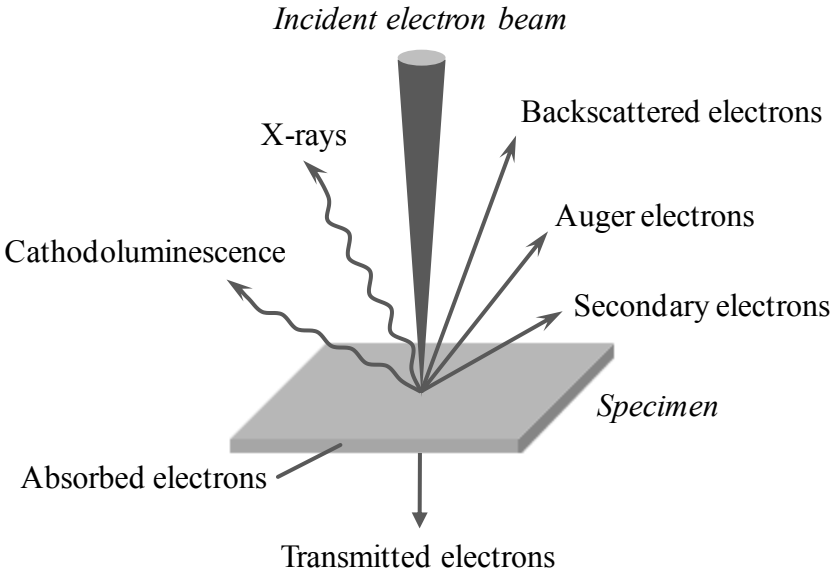

Figure 3.3 Emissions from solid specimen under the irradiation of high-energy electron beam.[5]

There are several emissions from the solid specimen when the high-energy electron beam irradiates this specimen (Figure 3.3).[5] The incident electrons dislodge secondary electrons from the specimen by transferring their energy to the specimen. Because of owning low energy, the secondary electrons generated at the surface of the specimen are emitted whereas the others generated at deeper regions are quickly absorbed. Therefore, the emitted secondary electrons are very sensitive to the surface of the specimen. The SEM technique detects these emitted secondary electrons for study of the relief of the surface.

Under the irradiation of the high-energy electron beam, the electrons in the inner shells of the atoms in the specimen are also emitted which leaves vacant orbits. The occupancy of these vacant orbits by the outer shell electrons results in the emission of X-ray photons whose energy corresponds to the energy difference between the outer shell electrons and the inner shell electrons. Therefore, the energy of the X-ray photons characterizes

individual elements, which allows the analysis of the composition of the specimen via EDS spectrum.

In TEM technique, the specimen must be thin enough to transmit the incident electrons. The interaction of the electrons with the specimen when it passes through allows projecting a real image of the specimen onto the viewing device.

3.4 X-ray photoelectron spectroscopy

X-ray photoelectron spectroscopy is the most widely used surface analysis technique.[6,7] The XPS measures the energy of electrons emitted from core levels (Figure 3.4). The binding energy of the electrons (E_B) can be calculated by following equation:

$$E_B = h\nu - E_K - \phi \qquad (3\text{-}4)$$

Where hν is the photon energy
E_K is the kinetic energy of the electron
ϕ is the spectrometer work function

Because the three quantities on the right-hand side the equation are measurable, it is easy to calculate the binding energy of the electrons.

The emitted electrons contribute to characteristic peaks in the XPS spectrum. The peaks of the electrons from p, d and f orbitals are split into two peaks due to the interaction of the electron angular momentum with the orbital angular momentum (Figure 3.5). Each electron has a quantum number associated with its spin angular momentum (s^2). The value of s can be either +1/2 or −1/2. The two angular momenta are added vectorially to produce the quantity j in the expression nl_j with $j = |l + s|$. The area ratio of the split peaks is equivalent to the ratio of the values $(2j + 1)$. For example, an electron from p orbital ($l = 1$) has two j values of 1/2 and 3/2, and thus the area ratio of the $p_{1/2}$ and $p_{3/2}$ peaks is 1:2 (Table 3.1).

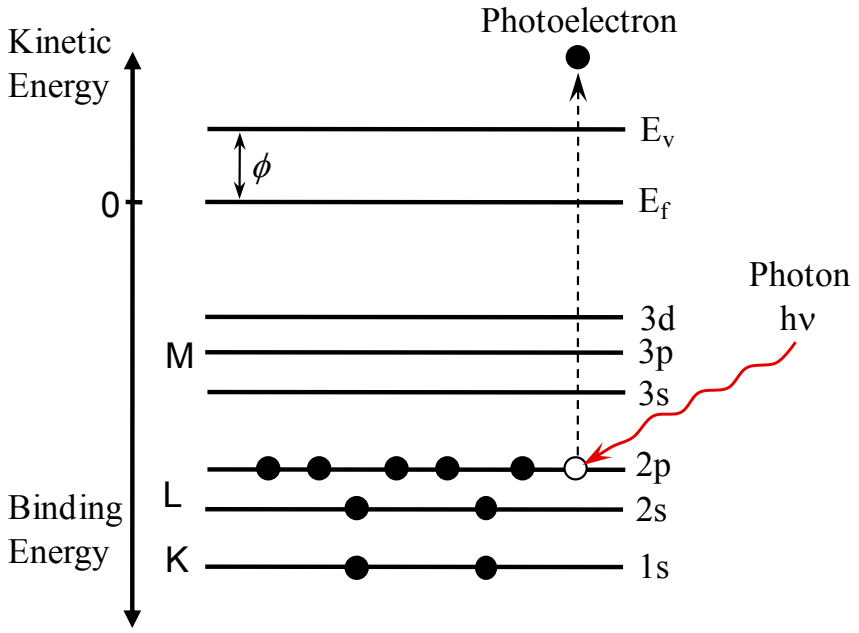

Figure 3.4 Schematic diagram of XPS process with the emission of an electron in 2p orbital.

Table 3.1 Summary for the splitting of core levels.

Orbital	j values	Area ratio $(2j_1 + 1) : (2j_2 + 1)$
s	1/2	
p	1/2, 3/2	1:2
d	3/2, 5/2	2:3
f	5/2, 7/2	3:4

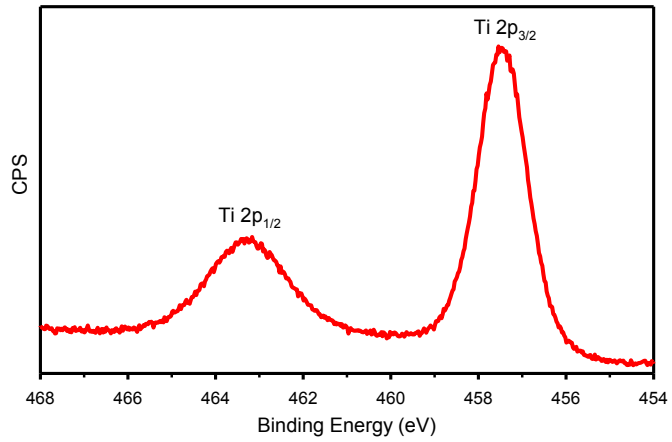

Figure 3.5 Example for the splitting of Ti 2p XPS peak into Ti $2p_{1/2}$ and Ti $2p_{3/2}$ peaks in TiO_2.

The binding energy identifies an electron specifically, both in terms of its parent element and atomic energy level. The change in the oxidation state and in the surroundings of an atom shifts the binding energy of the core electrons and this binding energy change is named chemical shift. In general, the removal of valence electrons increases the binding energy whereas the addition of valence electrons decreases the binding energy. Moreover, the binding enegy of the core levels increases when electrons are withdrawn from the atom by chemical bonding. Therefore, the chemical shift provides valuable information on the oxidation state, chemical environment and functional group.

3.5 Fourier transform infrared spectroscopy

The FTIR spectroscopy is used for investigation of the chemical bonds in materials by the excitation of the vibrations by the infrared radiation with frequencies in the range of 400 – 4000 cm^{-1}.[8] The vibrations are infrared active if the molecule has a permanent dipole moment or the dipole moment of the molecule changes during the oscillations (Table 3.2).[9] Each chemical bond with several vibrational modes can absorb several frequencies with different intensities. The stretching vibrations cause stronger absorptions of IR radiation rather than the bending vibrations (Figure 3.6). The absorbed frequencies are the characteristics of chemical bonds. Therefore, FTIR technique is suitable for identification of functional groups.

Table 3.2 Selection rules for Raman and infrared activity of vibrations.[9]

molecule	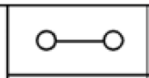	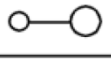	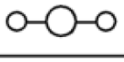		
vibration	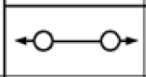	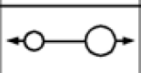	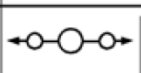	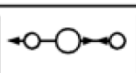	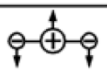
change of α with Q		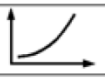	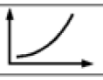	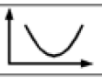	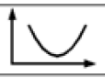
$\frac{d\alpha}{dQ}$	≠0	≠0	≠0	=0	=0
Raman active	yes	yes	yes	no	no
change of $\vec{P}_D$ with Q		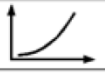	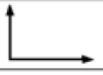	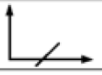	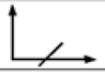
$\frac{d\vec{P}_D}{dQ}$	=0	≠0	=0	≠0	≠0
infrared active	no	yes	no	yes	yes

P_D for the dipole moment, α for the polarizability and Q for the normal coordinate of the molecule

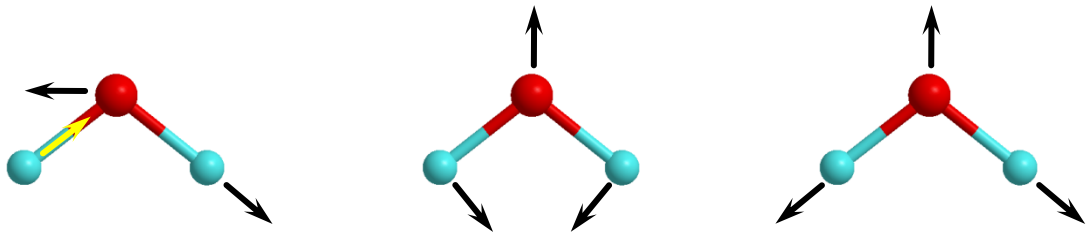

Asymmetric stretch Bend Symmetric stretch

Figure 3.6 Different vibrational modes of an asymmetric triatomic molecule.

3.6 Ultraviolet-visible spectroscopy

The solid state UV-vis spectroscopy is employed to characterize the absorbance of light of semiconductor photocatalysts.[10] The energy of photons in the visible region and the near ultraviolet region with the wavelength from 200 nm to 800 nm can excite electrons from the VB into the CB of a semiconductor. When a semiconductor is illuminated by light with

energy matching or exceeding that of the band gap of the semiconductor, the light induces the photoexcitation (Figure 3.7). The wavelength at which the light absorption occurs, together with the intensity of the absorption are recorded by an optical spectrometer and plotted in the form of UV-vis spectrum.

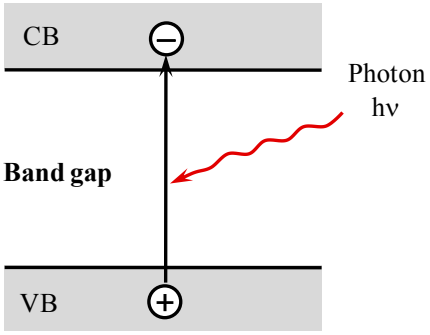

Figure 3.7 Schematic photoexcitation in semiconductor.

The band gap energy (E) of semiconductor can be calculated from the absorption edge on the UV-vis spectrum by following equation:

$$E = \frac{hc}{\lambda} \qquad (3\text{-}5)$$

Where h is Plank constant (6.626×10^{-34} J.s)

c is the speed of light (3.0×10^{8} m/s)

λ is wavelength at absorption edge (nm)

The conversion factor: $1eV = 1.6 \times 10^{-19}$ J

3.7 ζ-Potential analysis

The electrical state of a charged surface is determined by the spatial distribution of ions around it. The ionic distribution is called electrical double layer (EDL).[11] In a physical model, one layer of the EDL (Stern layer) is firmly bound to the particle as a fixed charge, while the other layer (diffuse layer) is loosely associated with the particle. The stern layer contains ions opposite in sign to the surface charge. The diffuse layer contains an excess of

counter-ions opposite in sign to the fixed charge, and a deficit of co-ions of the same sign as the fixed charge. As a result, the electrical potential is a function of the distance from the charged surface of the particle suspended in a medium (Figure 3.8). The potential at the slip plane is identified as ζ-potential.

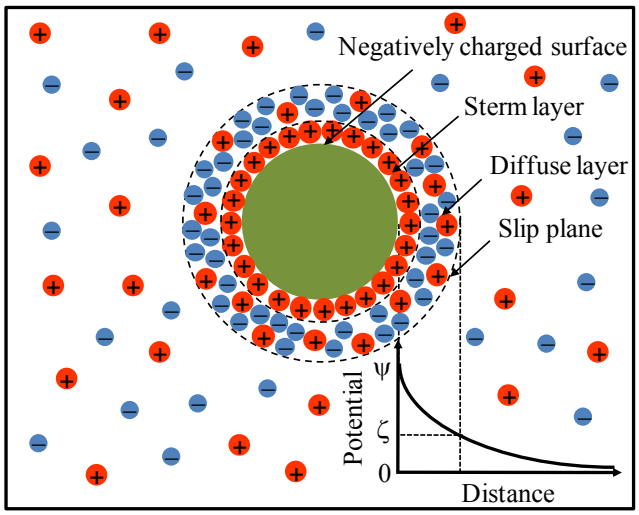

Figure 3.8 Scheme for the ionic distribution and electrical potential of a negatively charged particle.[12]

ζ-potential analysis is widely employed to identify the electrical charge of particles. The absolute value of ζ-potential implies the stability of a colloidal dispersion. Colloids with high ζ-potentials are electrically stable due to the strong repulsion of adjacent particles, whereas others with low ζ-potentials tend to an aggregation since the attraction between adjacent particles exceeds the repulsion.

3.8 Thermal analysis

Thermogravimetric analysis (TGA) quantifies the loss weight of sample as a function of increasing temperature.[13,14] The mass change with an increase in temperature gives valuable information about the removal of guest molecules as well as the stability of the material at certain temperature. The profile of the TGA thermogram can be used for calculating the amount of the components present in the sample.

The mass change of the materials is typically evoked by evaporation or decomposition of components, by oxidation or reduction. These processes are usually exothermic or endothermic. The complementary differential thermal analysis (DTA) allows identifying a process either exothermic or endothermic by recording temperature difference between the sample and an inert reference while both are subjected to the same heating program. Therefore, the thermal analysis techniques provide information relating to certain physical and chemical phenomena that occur during heating.

3.9 Elemental analysis

Elemental analysis for carbon is based on the conversion of all of the carbon in materials to CO_2 gas.[15] This analysis is carried out by a multistep process including the mineralization of the material in the presence of excess oxygen at high temperature about 1000 °C, the subsequent complete oxidation of the resulted gases mixture and the quantification of CO_2 gas. The amount of CO_2 gas after the process is determined by gas chromatography.

Atomic absorption spectroscopy is used for the qualitative and quantitative analysis of metal elements present in materials.[16] The technique is based on the absorption of light of free atoms in gaseous state. Electrons of the free atoms can be promoted to excited states for a short period of time by absorbing radiations. The atoms of each chemical element absorb a characteristic wavelength. This enables the qualitative analysis of a sample. The absorbance is proportional to the concentration of the element in the sample. Thus, the concentration can be calculated based on the Beer-Lambert law:

$$A = \log \frac{I_o}{I} \qquad (3\text{-}6)$$

Where A is absorbance

I_o is the intensity of the light passing through the reference

I is the intensity of the light passing through the sample

3.10 Gas sorption

3.10.1 Physisorption isotherm and surface area measurement.

One of the most important properties of MOFs is porosity. Adsorption-desorption isotherm analysis is widely used for determining their surface area, pore volume and pore size distribution.[17] The isotherm is the plot of adsorbed volume at the standard pressure against the corresponding equilibrium pressure (P/P_o) at a constant temperature.

There are six types of physisorption isotherm (Figure 3.9).[18,19] The reversible Type I isotherm is given by microporous materials in which the rapid rise at low pressures corresponds to monolayer adsorption, followed by a plateau because of the filling of the micropores. The reversible Type II and III isotherms are the normal forms obtained with non-porous or macroporous adsorbents. Type IV and V isotherms are characteristic of multilayer adsorption consisting of capillary condensation onto mesoporous materials. The Type V is uncommon isotherm relating to the Type III isotherm in that the adsorbent-adsorbate interaction is weak. Type VI isotherm is typical of stepwise multilayer adsorption on a uniform nonporous surface.

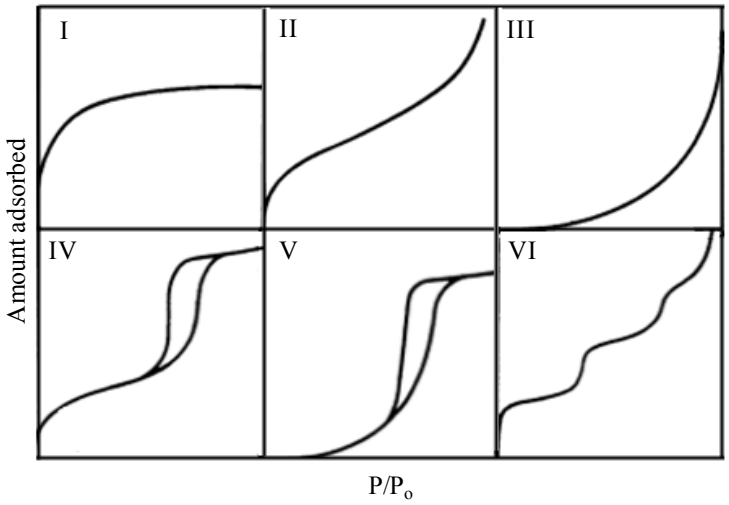

Figure 3.9 Types of physisorption isotherms.[18, 19]

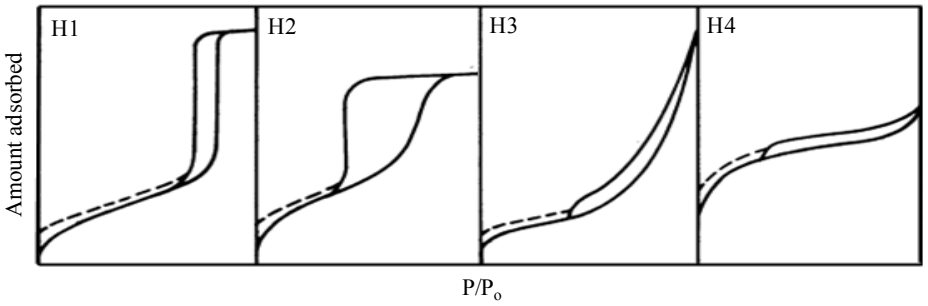

Figure 3.10 Types of hysteresis loops.[18, 19]

The characteristic of the Type IV isotherm is its hysteresis loop, *i.e.* the adsorption and desorption branches do not coincide in the multilayer range, which is associated with capillary condensation in mesopores. The hysteresis loops exhibit a wide variety of shapes (Figure 3.10). Type H1 hysteresis is a symmetrical loop consisting of almost vertical and nearly parallel adsorption/desorption branches. The type H1 is attributed to uniform cylindrical pores with a narrow pore size distribution. Type H2 is an asymmetrical loop consisting of a desorption branch much steeper than the adsorption branch. The type H2 is assigned to "ink-bottle" pores with narrow necks and wide bodies. Type H3 is associated with slit-shaped pores formed by the aggregate of plate-like particles. Type H4 with nearly horizontal and parallel branches over a wide range of P/P_o is often associated with narrow slit-like pores.

There are several theories to determine the surface area of porous materials. The most common theory is the Brunauer-Emmett-Teller (BET) model. The surface area is determined by using the BET equation:[20]

$$\frac{P/P_o}{n(1-P/P_o)} = \frac{1}{n_m c} + \frac{c-1}{n_m c} \times \frac{P}{P_o} \qquad (3\text{-}7)$$

Where n is the amount adsorbed at the relative pressure P/P_o

n_m is the monolayer capacity

c is a constant related exponentially to the heat of adsorption in the first adsorbed layer.

In practice, the c value is nearly taken as:

$$c = e^{(q_1 - q_L)/RT} \tag{3-8}$$

Where q_1 is the heat of adsorption of the first layer of gas molecules

q_L is the heat of the gas liquefaction

R and T are the gas constant and the absolute temperature, respectively.

The BET equation gives a linear relationship between $\frac{P/P_o}{n(1-P/P_o)}$ and P/P_o. The values of n_m and c are calculated from the intercept $\frac{1}{n_m c}$ and slope $\frac{c-1}{n_m c}$. The surface area can thus be calculated from the monolayer capacity on the assumption of close packing as:

$$A = n_m \alpha_m L \tag{3-9}$$

Where α_m is the molecular cross-sectional area

n_m is the monolayer capacity

L is the Avogadro constant

Generally, nitrogen is considered to be the most suitable gas for surface area determination and it is usually assumed that the BET monolayer is close-packed, giving $\alpha_m = 0.162$ nm^2 at 77 K.

3.10.2 Micropore analysis

Several methods have been established for micropore analysis. The common methods are t-plots, α_s-plots, Dubinin-Radushkevich (DR), Dubinin-Astakhov (DA), Horvath-Kawazoe (HK), Saito-Foley and the methods based on the density functional theory (DFT).

In this thesis, t-plot method has been used for the analysis of the volume and the surface area of micropores.[18] The method is based on t-curve that is the plot of the standard adsorbed amount with the statistical thickness of the adsorbed multilayer. The statistical thickness is calculated as the function of P/P_o in the range $0.45 < t < 1.0$ nm by using the de Boer equation:

$$t = \left[\frac{13.99}{0.034 - \log \frac{P}{P_o}} \right]^{1/2} \qquad (3\text{-}10)$$

The t-plot is a straight line that passes through the origin in the case of non-porous materials (Figure 3.11). If the material is microporous, the t-plot exhibits a positive intercept and the micropore volume can be calculated from this intercept. The slope, s, of the linear branch is proportional to the external surface area, *i.e.* the total area of the outside and pores that are not micropores, as following equation:

$$S_t = s \times 15.47 \qquad (3\text{-}11)$$

The constant 15.47 here represents the conversion of the gas volume to liquid volume.

The micropore surface area can be calculated as the differential between the total surface area S_{BET} and the external surface area S_t.

If the material contains mesopores, the capillary condensation will occur when the relative pressure reaches a value relating to the radius of the pore by the Kelvin equation. Therefore, the t-plot will show an upward deviation commencing at the relative pressure at which the finest pores are just being filled.

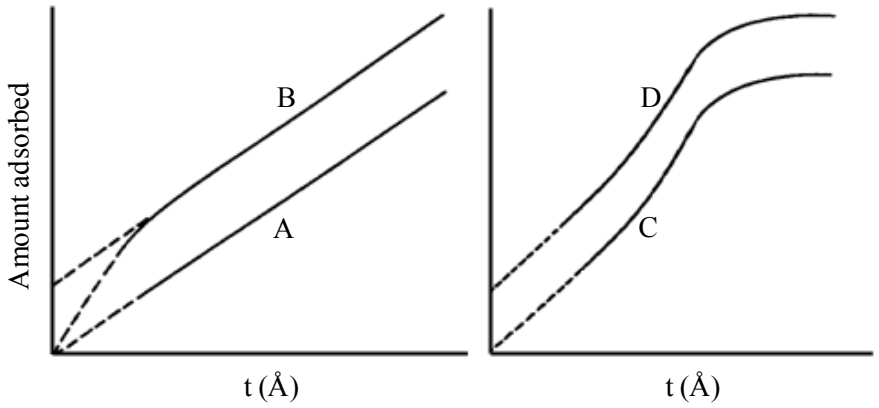

Figure 3.11 t-plots of non-porous (curve A), microporous (curve B), mesoporous (curve C) and bimodal micro-mesoporous (curve D) materials.[18]

The Horvath-Kawazoe method is used for the characterization of the size distribution of micropores.[21] The HK model yields a relation between pore filling pressure and the pore width from the free energy change of the adsorption because the adsorbate molecules transfer from the bulk gas phase to the adsorbed phase, through following equation:

$$\ln \frac{P_c}{P_o} = \frac{\phi(H)}{RT} \qquad (3\text{-}12)$$

Where P_o is the bulk gas saturation pressure

P_c is the pore filling pressure

ϕ is the heat of adsorption

H is the pore width

R is the gas constant

T is temperature.

3.10.3 Size distribution of mesopores

The size distribution of mesopores is estimated by using the Barrett-Joyner-Halenda (BJH) method on the desorption branch data based on the Kelvin equation:[22]

$$\ln \frac{P}{P_o} = -\frac{2\gamma V_m}{RT} \times \frac{1}{r_K} \qquad (3\text{-}13)$$

Where P/P_o is the relative pressure of vapor in equilibrium with a meniscus having a radius r_K (Kelvin radius)

γ and V_m are the surface tension and molar volume of liquid nitrogen at its boiling point

R and T are the universal gas constant and boiling point of nitrogen.

3.11 Gas chromatography analysis

Gas chromatography (GC) is an analytical separation technique used for identification of compounds that can be vaporized without decomposition from a complex mixture. The separation of gas phase molecules in GC system is a dynamic process that is based on the difference in the partitioning coefficients of the molecules over a moving mobile gas phase and a stationary phase. The higher the affinity with the stationary phase, the more a compound partitions into that phase and the longer it takes before it passes through the GC system.[23] As a result, the compounds are separated along GC column and reach the end of the column at different periods of time (so-called retention times). The compounds exiting the end of the column are identified and quantified by an appropriate electronic detector. The signal from the detector is related to their concentrations.